

Black hole evolution with the BSSN system by pseudo-spectral methods

Wolfgang Tichy

Department of Physics, Florida Atlantic University, Boca Raton, FL 33431

We present a new pseudo-spectral code for the simulation of evolution systems that are second order in space. We test this code by evolving a non-linear scalar wave equation. These non-linear waves can be stably evolved using very simple constant or radiative boundary conditions, which we show to be well-posed in the scalar wave case. The main motivation for this work, however, is to evolve black holes for the first time with the BSSN system by means of a spectral method. We use our new code to simulate the evolution of a single black hole using all applicable methods that are usually employed when the BSSN system is used together with finite differencing methods. In particular, we use black hole excision and test standard radiative and also constant outer boundary conditions. Furthermore, we study different gauge choices such as $1 + \log$ and constant densitized lapse. We find that these methods in principle do work also with our spectral method. However, our simulations fail after about $100M$ due to unstable exponentially growing modes. The reason for this failure may be that we evolve the black hole on a full grid without imposing any symmetries. Such full grid instabilities have also been observed when finite differencing methods are used to evolve excised black holes with the BSSN system.

PACS numbers: 04.25.Dm, 02.70.Hm, 04.70.Bw, 95.30.Sf

I. INTRODUCTION

Currently several gravitational wave detectors such as LIGO [1] or GEO [2] are already operating, while several others are in the planning or construction phase [3]. One of the most promising sources for these detectors are the inspirals and mergers of binary black holes. In order to make predictions about the final phase of such inspirals and mergers, fully non-linear numerical simulations of the Einstein Equations are required. In order to numerically evolve the Einstein equations, at least two ingredients are necessary. First we need a specific formulation of the evolution equations. And second, a particular numerical method is needed to implement these equations on a computer. For both these ingredients many choices are available. However, only a few of these choices have so far been successful in the evolution of a binary black hole system. In terms of commonly used evolution systems there is mainly the BSSN system [4] and also the generalized harmonic system [5]. The main numerical methods are finite differencing and spectral methods.

The original generalized harmonic system is second order and has only been used together with finite differencing techniques [5, 6, 7]. Yet, recently a first order version of this system has also been successfully evolved using a spectral method [8, 9]. Nevertheless, the majority of the astrophysically relevant binary black hole simulations to date have used one particular combination: The BSSN evolution system together with finite differencing techniques. With this choice, several groups have recently performed binary black hole simulations of one orbit or more [10, 11, 12, 13, 14, 15, 16]. However, the BSSN system has never before been tested with a spectral method. And in fact, no second order in space system such as BSSN has ever been tried together with a spectral method. Even for single black holes, only systems that are first order in time and space (such as the

KST system [17] or the first order version of the generalized harmonic system) have been used successfully with a spectral method. In order to derive such first order systems additional variables have to be introduced which have to satisfy additional constraints. It is therefore possible that second order systems perform better since they have fewer potentially unstable constraint violating solutions which can be excited due to numerical errors.

The aim of this paper is thus to test the standard BSSN system with its standard boundary conditions in a simple case but with a pseudo-spectral method. Such a test will show how well a spectral method will work when employed to this widely used and successful system. We will implement the BSSN system in its original second order in space form, without introducing any extra variables or constraints. This will also allow us to draw some conclusions about how well second order systems work when a spectral method is used. In order to perform this task we have developed the SGRID code, which can evolve second order in space systems using a pseudo-spectral collocation method. This code currently supports cubical or spherical domains and allows for spectral expansions in Fourier or Chebyshev basis.

Throughout we will use units where $G = c = 1$. The paper is organized as follows. In Sec. II we describe our methods and show results for some simple tests where we evolve non-linear scalar waves. Sec. III describes our particular implementation of BSSN and presents tests for case of a single black hole. We conclude with a discussion of our results in Sec. IV.

II. DESCRIPTION OF OUR METHOD AND CODE TESTS

In this section we describe the methods we use in the SGRID code we have developed. Furthermore, we present some code tests with scalar wave equations.

A. The pseudo-spectral collocation method

In one spatial dimension, spectral methods are based on expansions

$$u(X) = \sum_{l=1}^N \tilde{a}_l A_l(X) \quad (1)$$

of every evolved field $u(X)$ in terms of suitable basis functions $A_l(X)$ with coefficients \tilde{a}_l . Once the coefficients are known it is easy to compute derivatives of $u(X)$ from

$$\partial_X u(X) = \sum_{l=1}^N \tilde{a}_l \partial_X A_l(X), \quad (2)$$

since the derivatives of the basis functions are known analytically.

However, instead of directly storing and manipulating the coefficients \tilde{a}_l up to some desired order N in l , we make use of the fact that (for the basis functions of interest) we can derive \tilde{a}_l from the values of $u(X)$ at certain collocation points. If $u(X)$ is known to have the values $u(X_i) = u_i$ at the collocation points X_i for $i = 1, 2, \dots, N$ it is possible to invert the N equations

$$u_i = \sum_{l=1}^N \tilde{a}_l A_l(X_i) \quad (3)$$

and to exactly solve for the N coefficients \tilde{a}_l in terms of the u_i . The location of the different collocation points depends on the basis functions used. For example, for Fourier expansions the collocation points have to be equally spaced in the X -interval considered.

This approach of storing the field's values u_i at the collocation points is called a pseudo-spectral collocation method. This method has the advantage that non-linear terms such as $u(X_i)^2$ can be computed from simple multiplications. Also, the fields at each point can be evolved forward in time by a simple method of lines integrator such as Runge-Kutta or iterative Crank-Nicholson (ICN).

The generalization to 3 dimensions, is straight forward and can be summarized by

$$u(X_i, Y_j, Z_k) = \sum_{l,m,n} \tilde{d}_{lmn} A_l(X_i) B_m(Y_j) C_n(Z_k). \quad (4)$$

I.e. we are using basis functions which are products of functions that depend only on one coordinate. Note that the three coordinates X , Y and Z need not be Cartesian coordinates.

For this, paper we we have chosen X , Y and Z to be the spherical coordinates r , θ and ϕ . I.e. standard Cartesian coordinates are given by

$$x = r \sin(\theta) \cos(\phi) \quad (5)$$

$$y = r \sin(\theta) \sin(\phi) \quad (6)$$

$$z = r \cos(\theta). \quad (7)$$

As basis functions we will use the Chebyshev polynomials

$$A_l(r_i) = \cos \left(l \arccos \left(\frac{2r_i - R_{out} - R_{in}}{R_{in} - R_{out}} \right) \right) \quad (8)$$

in the radial direction, where R_{in} and R_{out} stand for the inner and outer radii of our numerical domain. For the angular directions we use the Fourier basis

$$B_m(\theta_j) = \frac{1}{N_\theta} e^{-im\theta_j} \quad (9)$$

and

$$C_n(\phi_k) = \frac{1}{N_\phi} e^{-in\phi_k}. \quad (10)$$

The collocation points are chosen to be

$$r_i = \frac{R_{in} - R_{out}}{2} \cos \left(\frac{i\pi}{N_r - 1} \right) + \frac{R_{in} + R_{out}}{2} \quad (11)$$

$$\theta_j = \pi(2j + 1)/N_\theta \quad (12)$$

$$\phi_k = 2\pi k/N_\phi, \quad (13)$$

where

$$i = 0, 1, \dots, N_r - 1, \quad (14)$$

$$j = 0, 1, \dots, N_\theta - 1 \quad (15)$$

$$k = 0, 1, \dots, N_\phi - 1. \quad (16)$$

Any function $u(r, \theta, \phi)$ can then be expressed in this basis as

$$u(r_i, \theta_j, \phi_k) = \sum_{l=0}^{N_r-1} \sum_{m=0}^{N_\theta-1} \sum_{n=0}^{N_\phi-1} \tilde{d}_{lmn} A_l(r_i) B_m(\theta_j) C_n(\phi_k). \quad (17)$$

However, in our code we never really uses this expansion to compute all the coefficients \tilde{d}_{lmn} . Rather, we only ever expand in one direction and instead use

$$u(r_i, \theta_j, \phi_k) = \sum_{l=0}^{N_r-1} \tilde{a}_l(\theta_j, \phi_k) A_l(r_i), \quad (18)$$

$$u(r_i, \theta_j, \phi_k) = \sum_{m=0}^{N_\theta-1} \tilde{b}_l(r_i, \phi_k) B_m(\theta_j), \quad (19)$$

$$u(r_i, \theta_j, \phi_k) = \sum_{n=0}^{N_\phi-1} \tilde{c}_l(r_i, \theta_j) C_n(\phi_k), \quad (20)$$

to compute the coefficients $\tilde{a}_l(\theta_j, \phi_k)$, $\tilde{b}_l(r_i, \phi_k)$ or $\tilde{c}_l(r_i, \theta_j)$ along a line in the r -, θ - or ϕ -direction. As

we will see, this suffices to compute partial derivatives in any coordinate direction.

Note that we always choose N_θ to be even, in order to assure that collocation points in the θ -direction (see Eq. (12)) do not occur at $\theta = 0$ and $\theta = \pi$. In this way the coordinate singularities at the poles are avoided. Notice that, since both θ and ϕ are between 0 and 2π , we have a double covering of the entire domain. This double covering is due to the fact that we use Fourier expansions in both angles.

Spherical coordinates also have a coordinate singularity at $r = 0$. In this paper we avoid this singularity by simply choosing $R_{in} > 0$ so that r_i in Eq. (11) is always larger than zero. This is the appropriate choice for simulating a single black hole using excision. From Eq. (11) and we see that the collocation points for $i = 0$ and $i = N_r - 1$ are located on the inner and outer boundaries of the numerical domain. Hence it is straightforward to impose boundary conditions there.

B. Results for non-linear scalar waves

In order to test our approach we have performed tests with a non-linear wave equation for a scalar field ψ . When written as a first order in time and second order in space system, the evolution equations in Cartesian coordinate are

$$\partial_t \psi = \Pi \quad (21)$$

$$\partial_t \Pi = (\partial_x^2 + \partial_y^2 + \partial_z^2)\psi - \lambda \frac{\psi^3}{1 + \psi^2}, \quad (22)$$

where λ parametrizes the non-linearity. This is also how we have implemented this equation in our computer code, with the caveat that the Cartesian derivatives are computed using the expansions (18), (19) and (20). By this we mean that before each timestep derivatives like $\partial_x \psi$ are computed using

$$\partial_x \psi = \frac{\partial r}{\partial x} \partial_r \psi + \frac{\partial \theta}{\partial x} \partial_\theta \psi + \frac{\partial \phi}{\partial x} \partial_\phi \psi, \quad (23)$$

where $\partial_r \psi$, $\partial_\theta \psi$ and $\partial_\phi \psi$ can easily be obtained from the expansions in Eqs. (18), (19) and (20) since the derivatives of $A_l(r)$, $B_m(\theta)$ and $C_n(\phi)$ are known analytically. In order to evolve forward in time we can use any method of lines integrator. In this paper we will only present results obtained with a second order in time ICN scheme. We have, however, also implemented and tested several different Runge-Kutta schemes. In terms of stability all these integrators work equally well for the cases discussed below, so that the ICN results suffice for our purposes.

The numerical domain for the scalar wave test is a spherical shell with an inner radius of $R_{in} = 2$ and an outer radius of $R_{out} = 52$. Since the grid points are equally spaced in θ and ϕ , the smallest grid spacings occur near the poles in the ϕ -direction. This smallest

grid spacing is of order

$$h \sim R_{in} \frac{2\pi^2}{N_\theta N_\phi}. \quad (24)$$

In order to not violate the Curret condition the time step Δt has to be chosen to be of order h as well. This means that we have to take very small time steps, so that the simulations take longer. But it also means that the error in the ICN time integrator will be only of order $\Delta t^2 \sim h^2 \sim (N_\theta N_\phi)^{-2}$.

As boundary condition at $r = R_{in}$ we always use

$$u(t, R_{in}, \theta, \phi) = u(t = 0, R_{in}, \theta, \phi), \quad (25)$$

where u stands for either ψ or Π . At $r = R_{out}$ we have tested both the constant boundary condition

$$u(t, R_{out}, \theta, \phi) = u(t = 0, R_{out}, \theta, \phi) \quad (26)$$

and also the radiative boundary condition

$$\begin{aligned} \partial_t u(t, R_{out}, \theta, \phi) = -v \Big[& \frac{u(t, R_{out}, \theta, \phi)}{r} \\ & + \frac{x}{r} \partial_x u(t, R_{out}, \theta, \phi) \\ & + \frac{y}{r} \partial_y u(t, R_{out}, \theta, \phi) \\ & + \frac{z}{r} \partial_z u(t, R_{out}, \theta, \phi) \Big]. \end{aligned} \quad (27)$$

For our scalar field example we use $v = 1$, and apply this boundary condition to both ψ and Π directly, without decomposing ψ and Π into incoming and outgoing modes at the boundaries.

As initial data for the scalar field we use an inward moving Gaussian profile given by

$$\psi = \frac{A}{r} e^{-\frac{(x-x_0)^2}{2\sigma_x^2} - \frac{(y-y_0)^2}{2\sigma_y^2} - \frac{(z-z_0)^2}{2\sigma_z^2}}, \quad (28)$$

$$\begin{aligned} \Pi = & -\frac{A}{r} e^{-\frac{(x-x_0)^2}{2\sigma_x^2} - \frac{(y-y_0)^2}{2\sigma_y^2} - \frac{(z-z_0)^2}{2\sigma_z^2}} \\ & \left[\frac{(x-x_0)x}{\sigma_x^2 r} + \frac{(y-y_0)y}{\sigma_y r} + \frac{(z-z_0)z}{\sigma_z^2 r} \right], \end{aligned} \quad (29)$$

where

$$A = 1, \quad x_0 = 27, \quad y_0 = z_0 = 0, \quad \sigma_x = 4, \quad \sigma_y = \sigma_z = 10 \quad (30)$$

Figure 1 shows the scalar field energy E_ψ inside our numerical domain, computed from a volume integral over the energy density

$$\begin{aligned} \rho = & \frac{\Pi^2}{2} + \frac{(\partial_x \psi)^2 + (\partial_y \psi)^2 + (\partial_z \psi)^2}{2} \\ & + \frac{\lambda}{2} [\psi^2 - \log(1 + \psi^2)]. \end{aligned} \quad (31)$$

The plot shows E_ψ for different outer boundary conditions and also for different λ . The dotted line shows the

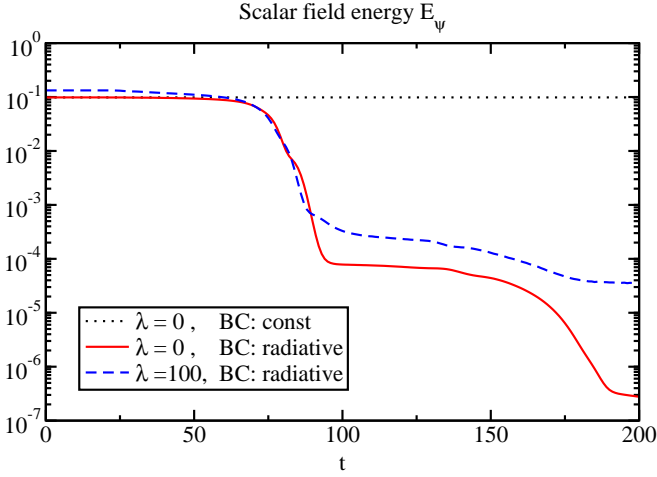


FIG. 1: The plot shows the scalar field energy inside our numerical domain for three different cases. If the fields are kept constant at the outer boundary no energy can leave the domain and thus the energy remains constant (dotted line). If we use the radiative outer boundary condition (27), waves can leave the domain and thus the energy decreases over time. The solid line shows this decrease for the linear ($\lambda = 0$) case, while the broken line depicts the non-linear case ($\lambda = 100$). In all three cases we have used $N_r = N_\theta = 30$ and $N_\phi = 29$.

result if we use $\lambda = 0$, together with the outer boundary condition (26). In that case the resulting linear waves are reflected by the boundaries so that the energy remains constant. The solid line depicts the $\lambda = 0$ case with the radiative outer boundary condition (27). Since the initial wave profile is moving inward, it takes about one crossing time until the wave starts leaving the grid. After that (around $t \sim 100$) the energy starts dropping. The same qualitative behavior occurs in the non-linear case for $\lambda = 100$. Note that even though we used identical initial data in all cases, the energy E_ψ in the non-linear case is initially about 35% larger. Thus for $\lambda = 100$ the non-linear terms are not negligible and are by no means a small perturbation. This means that the simple radiative outer boundary condition (27) is not only capable of propagating non-linear waves off the grid, it also does not seem to lead to any instabilities in the scalar wave tests performed by us. This result is interesting since an analogous outer boundary condition is also used in almost all stable black hole evolution codes which use the BSSN system together with a finite differencing method.

In Fig. 2 we demonstrate that our code exhibits the expected geometric convergence if we increase the number of grid points. We show the error in E_ψ at $t = 200$, for the the non-linear wave equation with radiative outer boundary condition. Since no analytical solution was available to us, the error in the energy plotted here is defined by

$$\delta_{N,40}(E_\psi) = |E_{\psi,N} - E_{\psi,40}|, \quad (32)$$

where $E_{\psi,N}$ is the N th order spectral approximation to E_ψ obtained by using $N_r = N_\theta = N_\phi + 1 = N$. In Fig. 3

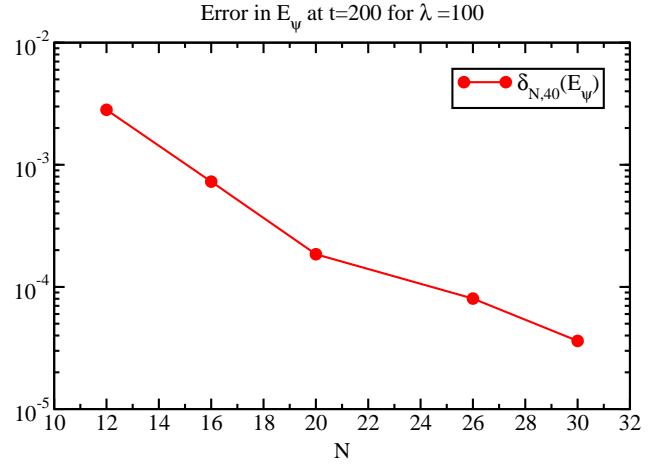


FIG. 2: This plot shows the error in E_ψ at $t = 200$, for the non-linear wave equation with the radiative outer boundary condition. One can see that the error decreases exponentially with the number of grid points N .

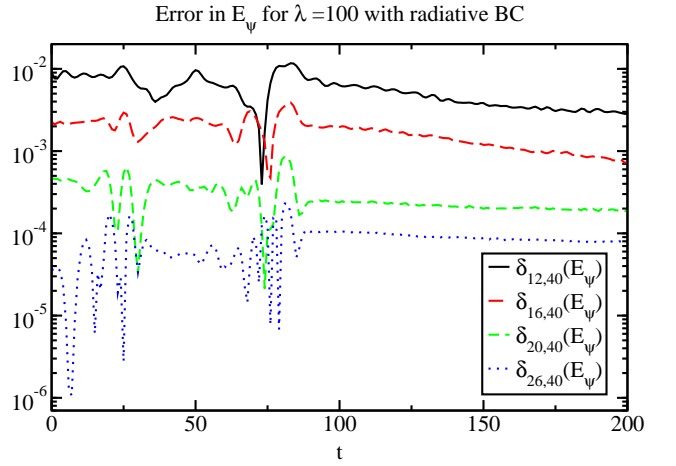


FIG. 3: This plot shows the error in E_ψ versus time, for the the non-linear wave equation with the radiative outer boundary condition.

we show the time evolution of this error. We can clearly see how the error decreases with an increasing N . Figure 4 shows the scalar field itself at time $t = 55$ along the ϕ -direction, for $r = 27$ and $\theta = \pi/2$. This time was chosen such that possible noise from the inner and outer boundaries has had time to reach $r = 27$. Also note that during that time the wave which was initially localized around $(r = 27, \theta = \pi/2, \phi = 0)$ has had time to reach the point $(r = 27, \theta = \pi/2, \phi = \pi)$. We see that for $N = 12$ points the wave still looks quite jagged, but it converges to a smooth result for higher N .

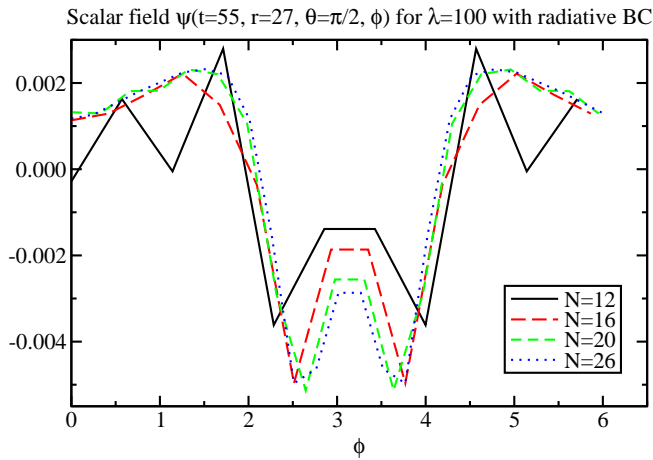


FIG. 4: This plot shows the scalar field ψ along an equatorial circle ($\theta = \pi/2$) with radius $r = 27$. Shown are snapshots of ψ at $t = 55$ for different numbers of grid points $N_r = N_\theta = N_\phi + 1 = N$.

C. Analysis of the well-posedness of the scalar wave boundary conditions

As already mentioned the boundary conditions used above are standard, in the sense that they have been used in almost all black hole simulations with the BSSN system so far. Like in the scalar field example above, they are applied to all evolved fields of the BSSN system, without decomposing them into incoming or outgoing modes at the boundary. Because of this it is not immediately obvious whether these boundary conditions are mathematically well-posed. However, at least in the scalar field case well-posedness can be demonstrated easily.

Scalar wave equations of the form (21) and (22) are well studied. For the sake of completeness we will here quote some results of Gundlach and Martin-Garcia [18] who have studied the well-posedness of systems that are first order in time and second order in space. First note that the non-linearity in Eq. (22) does not affect well-posedness. Hence our Eqs. (21) and (22) are completely analogous to Eqs. (1) and (2) in [18]. According to [18], the second order characteristic variables for direction n_i are given by

$$U_\pm = \Pi \pm \partial_n \psi \quad (33)$$

$$U_A = \partial_A \psi, \quad (34)$$

where ∂_n is the derivative in direction n_i and ∂_A are the derivatives normal to n_i . Here U_+ and U_- are the incoming and outgoing modes, while the U_A are zero speed modes. By using energy estimates, Gundlach and Martin-Garcia [18] show that the problem is well-posed if boundary conditions of the form

$$U_+ = \kappa U_- + f \quad (35)$$

are imposed on the incoming mode only, where $|\kappa| \leq 1$ and f is a given function.

We will now show that the boundary conditions (26) and (27) lead to a condition of the form (35).

Let us start with condition (26) and assume that our initial data satisfy $\Pi(t = 0, R_{out}, \theta, \phi) = \psi(t = 0, R_{out}, \theta, \phi) = 0$. Then Eq. (26) leads to $\Pi(t, R_{out}, \theta, \phi) = 0$ and $\psi(t, R_{out}, \theta, \phi) = 0$. Now $\Pi(t, R_{out}, \theta, \phi) = 0$ is completely equivalent to Eq. (35) for $\kappa = -1$ and $f = 0$. So if we had only this one boundary condition, the problem would certainly be well posed. In this case we should compute ψ at the boundary by using the evolution equation (21). However, if we do so, we immediately obtain that $\psi(t, R_{out}, \theta, \phi) = 0$, since $\Pi(t, R_{out}, \theta, \phi) = 0$. Thus imposing $\psi(t, R_{out}, \theta, \phi) = 0$ is redundant but completely consistent with the evolution equations. Hence our boundary condition (26) is equivalent to the well posed condition (35) with $\kappa = -1$ and $f = 0$. Note that in our actual numerical simulations we have really set $\Pi(t = 0, R_{out}, \theta, \phi) = \psi(t = 0, R_{out}, \theta, \phi) = 0$. I.e. at the boundary we do not really have a Gaussian profile. However, since our Gaussian is numerically almost indistinguishable from zero at the boundary anyway, any discontinuities introduced by this procedure are well below our numerical accuracy.

Next consider the radiative condition (27). For ψ it implies $\partial_t \psi = -[\partial_n \psi + \psi/R_{out}]$. If we use only this condition for ψ together with the evolution equation (21), we can replace $\partial_t \psi$ by Π . In this case we can compute ψ from the evolution equation (21) and our only boundary condition is

$$\Pi = -[\partial_n \psi + \psi/R_{out}]. \quad (36)$$

This boundary condition, however, is again of the form (35) with $\kappa = 0$ and $f = -\psi/R_{out}$. Thus in this case the problem would be well posed.

Now, the second condition coming from Eq. (27), i.e.

$$\partial_t \Pi = -[\partial_n \Pi + \Pi/R_{out}] \quad (37)$$

is already implied by the above procedure of using only the boundary condition (36) together with the evolution equation (21). (To arrive at Eq. (37) we can simply take the time derivative of Eq. (36) and use Eq. (21) to replace time derivatives of ψ .) Hence the radiative conditions (27) are simply an alternate but equivalent way of setting the fields at the boundary. Since this alternate way can be derived from the well-posed boundary condition (36), it is also well-posed.

In summary, the constant as well as the radiative boundary conditions of Eqs. (26) and (27) are both equivalent to imposing conditions only on the incoming scalar wave modes. Thus the scalar wave system is well-posed with either one of the two boundary conditions.

III. EVOLVING A SINGLE BLACK HOLE WITH THE BSSN SYSTEM

After having demonstrated that our methods lead to stable and convergent results for scalar waves we will now

turn to evolving a single black hole example using the BSSN system [4].

In the case of BSSN, the 3-metric g_{ij} is written as

$$g_{ij} = e^{4\phi} \tilde{\gamma}_{ij} \quad (38)$$

where the conformal metric $\tilde{\gamma}_{ij}$ has unit determinant. In addition, the extra variable

$$\tilde{\Gamma}^i = \tilde{\gamma}^{ij} \tilde{\gamma}^{kl} \tilde{\gamma}_{jk,l} \quad (39)$$

is introduced where $\tilde{\gamma}^{ij}$ is the inverse of the conformal metric. Furthermore, the extrinsic curvature is split into its trace free part \tilde{A}_{ij} and its trace K , and given by

$$K_{ij} = e^{4\phi} \left(\tilde{A}_{ij} + \frac{K}{3} \tilde{\gamma}_{ij} \right). \quad (40)$$

In terms of these variables the evolution equation are

$$\partial_t \tilde{\gamma}_{ij} = -2\alpha \tilde{A}_{ij} + \mathcal{L}_\beta \tilde{\gamma}_{ij} \quad (41)$$

$$\partial_t \phi = \frac{1}{6} (-\alpha K + D_i \beta^i) \quad (42)$$

$$\begin{aligned} \partial_t \tilde{\Gamma}^i = & -2\alpha \left(\frac{2}{3} \tilde{\gamma}^{ij} D_j K - 6 \tilde{A}^{ij} D_j \phi - \tilde{\Gamma}_{jk}^i \tilde{A}^{jk} \right) \\ & - 2 \tilde{A}^{ij} D_j \alpha - \xi (\tilde{\Gamma}^i - \tilde{\gamma}^{jk} \tilde{\Gamma}_{jk}^i) \beta_{,l}^l + \tilde{\gamma}^{jk} \beta_{,jk}^i v \\ & + \frac{1}{3} \tilde{\gamma}^{ij} \beta_{,kj}^k - \tilde{\Gamma}^j \beta_{,j}^i + \frac{2}{3} \tilde{\Gamma}^i \beta_{,k}^k + \beta^j \tilde{\Gamma}_{,j}^i \end{aligned} \quad (43)$$

$$\begin{aligned} \partial_t \tilde{A}_{ij} = & e^{-4\phi} \left[-D_i D_j \alpha + \alpha (\tilde{R}_{ij} + R_{ij}^\phi) \right]^{TF} \\ & + \alpha (K \tilde{A}_{ij} - 2 \tilde{A}_{ik} \tilde{A}_j^k) + \mathcal{L}_\beta \tilde{A}_{ij} \end{aligned} \quad (44)$$

$$\partial_t K = -D^i D_i \alpha + \alpha \left(\tilde{A}^{ij} \tilde{A}_{ij} + \frac{1}{3} K^2 \right) + \mathcal{L}_\beta K. \quad (45)$$

Here the superscript TF in Eq. (44) denotes the trace free part and D_i is the derivative operator compatible with the 3-metric g_{ij} . Notice that $\tilde{\Gamma}_{jk}^i$ and \tilde{R}_{ij} are the Christoffel symbol and Ricci tensor associated with the conformal metric $\tilde{\gamma}_{ij}$, while

$$\begin{aligned} R_{ij}^\phi = & -2 \tilde{D}_i \tilde{D}_j \phi - 2 \tilde{\gamma}_{ij} \tilde{D}^l \tilde{D}_l \phi \\ & + 4 (\tilde{D}_i \phi) (\tilde{D}_j \phi) - 4 \tilde{\gamma}_{ij} (\tilde{D}^l \phi) (\tilde{D}_l \phi), \end{aligned} \quad (46)$$

where \tilde{D}_i is the derivative operator compatible with the conformal metric $\tilde{\gamma}_{ij}$. For all the results reported here we have set the constant ξ in Eq. (43) to $\xi = 4/3$.

We should also note that in order to ensure that \tilde{A}_{ij} remains traceless during our numerical evolution, we subtract any trace due to numerical errors after each evolution step from \tilde{A}_{ij} .

As initial data we use the metric and extrinsic curvature of a Schwarzschild black hole of mass M in Kerr-Schild coordinates. Thus initially we have

$$g_{ij} = \delta_{ij} + 2H l_i l_j \quad (47)$$

$$\begin{aligned} K_{ij} = & \alpha [l_i H_{,j} + l_j H_{,i} + H l_{i,j} + H l_{j,i} \\ & + 2H^2 (l_i l_k l_{j,k} + l_j l_k l_{i,k}) + 2H l_i l_j l_k H_{,k}], \end{aligned} \quad (48)$$

where

$$\begin{aligned} H &= M/r \\ l^i &= x^i/r. \end{aligned} \quad (49)$$

The indices of l^i can be lowered with the flat metric.

As initial lapse and shift we use

$$\alpha = 1/\sqrt{1+2H}, \quad (50)$$

$$\beta^i = 2l^i H/(1+2H). \quad (51)$$

If this lapse and shift are kept constant during the evolution the right hand sides of Eqs. (41)-(45) are all zero and thus all the BSSN variables are constant. All the results presented in this paper are indeed obtained with a constant shift equal to what is given in Eq. (51). The lapse, however, is treated somewhat differently and we have tried two approaches. Firstly, following [19, 20, 21, 22] we have experimented with a so called 1+log-lapse given by

$$\partial_t \alpha = D_i \beta^i - \alpha K. \quad (52)$$

The second approach is to introduce a densitized lapse given by

$$q = \frac{\alpha}{\sqrt{g}}, \quad (53)$$

where g is the determinant of the 3-metric. As in [22] this densitized lapse q is then evolved instead of α , which is simply computed using Eq. (53). In our particular case we impose

$$\partial_t q = 0, \quad (54)$$

and thus we keep the densitized lapse constant during the evolution. Analytically both Eq. (52) and Eq. (54) lead to a constant lapse for the Kerr-Schild initial data used here. However, as we will see below, numerically both cases differ.

The BSSN system of evolution equations (Eqs. (41)-(45)) is first order in time and second order in space, just as the scalar wave example considered before. We will thus use the same numerical methods. As our numerical domain we use a spherical shell, which extends from $R_{in} = 1.85M$ to $R_{out} = 16M$, with collocation points given by Eqs. (11)-(13). On this shell we will use the Chebyshev basis (8) in the radial direction and the Fourier basis (9) and (10) in the angular directions. As before, we will evolve the Cartesian components of all variables on this spherical grid without rewriting the evolution equations in spherical coordinates.

The horizon of the black hole is at $r = 2M$, so that the inner boundary at $r = R_{in} = 1.85M$ is inside the horizon, which justifies excising the region $r < R_{in}$. We treat this inner boundary like a pure outflow boundary and do not impose any boundary condition there. Apart from using a spectral method this is the one point where we really have to do something that differs from what

is usually done when the BSSN system is evolved using finite differencing methods. Almost all finite differencing BSSN simulations performed so far either avoid excision altogether or, if excision is used, apply the so called “simple excision” boundary condition [20], where the time derivatives of variables at the inner boundary are obtained by copying the time derivatives from neighboring grid points. Even though one might worry about spoiling geometric convergence, this “simple excision” algorithm can in principle also be applied within our spectral method using collocation points. The results, however, are disastrous and the simulation crashes after only a few M of evolution time. In the continuum limit the “simple excision” technique corresponds to a Von Neumann boundary condition, which can also be applied within our spectral approach. This inner boundary condition, however, also leads to exponential blow up after only a few M of evolution time. Hence the simplest prescription which can be used without decomposing our variables into incoming and outgoing modes, is to impose no boundary condition at $r = R_{in}$. Fortunately this option is easily implemented within our spectral approach, and amounts to treating the points at $r = R_{in}$ in the same way as interior points by simply using the BSSN evolution equations at these points as well.

At the outer boundary at $r = R_{out} = 16M$ we have experimented with both constant and radiative boundary conditions. In the constant case we simply apply Eq. (26) to all evolved variables. Analytically this is the correct boundary condition since with our choices for lapse and shift nothing should evolve, so that all fields indeed remain constant at the boundary. We have also tested radiative boundary conditions. Following [21] we have applied a modified radiative boundary condition to our evolved variables. The modification consists of applying condition (27) to the difference between the evolved variables and the analytic solution given by the initial data. As in [21] we have applied this modified radiative boundary condition to all variables except $\tilde{\Gamma}^i$, which was kept constant at the outer boundary.

In the following we will present results for three different combinations of the boundary conditions and lapse choices described above. In Fig. 5 we show the ADM mass (see e.g. [23]) versus time. In principle the ADM mass should stay constant for all time. However, due to exponentially growing instabilities all our runs eventually crash and the ADM mass becomes more and more inaccurate over time. The two dashed lines are obtained when we use the radiative outer boundary conditions described above. The short dashed line is for the $1 + \log$ lapse of Eq. (52). This simulation lasts the longest. The long dashed line corresponds to a simulation where the densitized lapse of Eq. (53) is kept constant. The solid line is for a constant densitized lapse together with constant outer boundary conditions. This simulation crashes at about the same time as the corresponding one with radiative boundary conditions (long dashed line).

Let us discuss next how these results depend on the

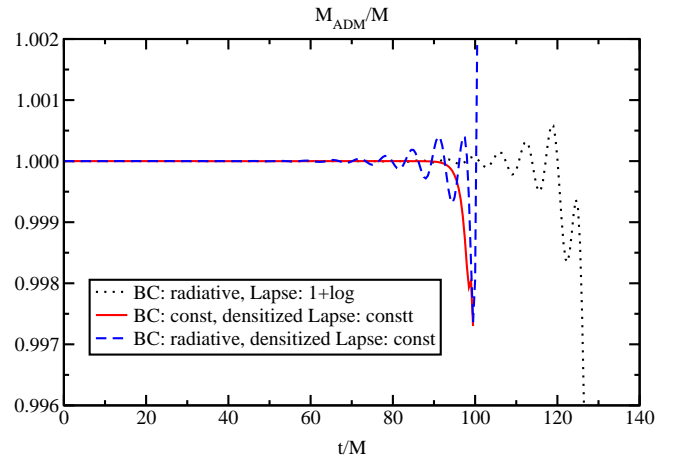


FIG. 5: ADM mass versus time for different choices of lapse and outer boundary conditions. The short dashed line is for the radiative outer boundary condition together with a $1 + \log$ lapse. This simulation crashes at $t = 137M$. The solid line depicts the result when all variables are kept constant at the outer boundary and a constant densitized lapse is used. In this case the run dies at $t = 99M$. The long dashed line shows the case for the radiative boundary condition together with a constant densitized lapse. Here a crash occurs at $t = 100M$. All results shown in this figure were obtained using $N_r = 30$, $N_\theta = 14$ and $N_\phi = 13$.

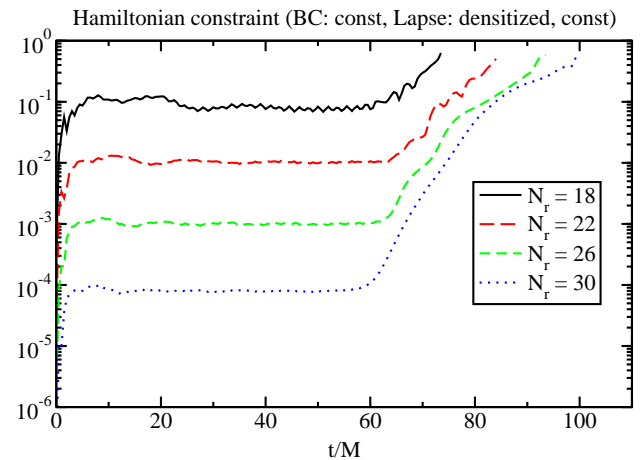


FIG. 6: The plot shows the L^2 -norm over the entire grid of the normalized Hamiltonian constraint versus time for the case of constant outer boundary conditions and a constant densitized lapse. In this plot $N_\theta - 1 = N_\phi = 13$. For increasing N_r we observe geometric convergence in the Hamiltonian until $t \sim 60M$.

resolution used. To this end it is instructive to study the normalized Hamiltonian constraint at different resolutions. Figure 6 shows the Hamiltonian for an increasing number of radial grid points N_r in the case of constant outer boundary conditions and a constant densitized lapse. After an initial increase in the Hamiltonian for the first few M , the curves become flat until instabilities take over at around $t \sim 60M$. These instabilities

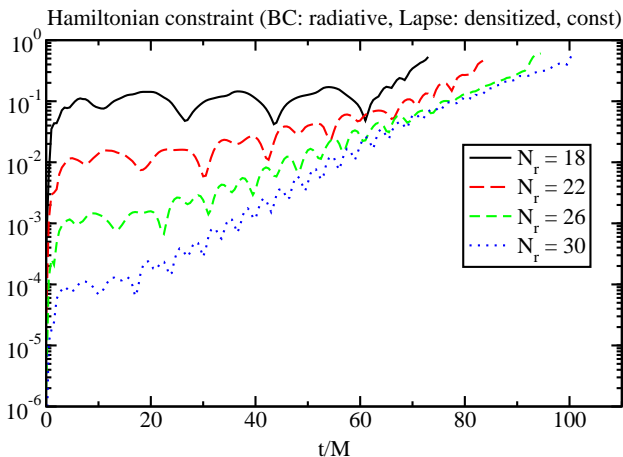


FIG. 7: The L^2 -norm of the normalized Hamiltonian constraint versus time for the case of radiative outer boundary conditions and a constant densitized lapse. For increasing N_r the Hamiltonian converges until about $t \sim 60M$. The angular resolution is $N_\theta - 1 = N_\phi = 13$.

eventually lead to a crash. We obtain geometric convergence until about $t \sim 60M$. Note that the simulations last longer when the resolution is increased.

In Fig. 7 we show the corresponding results for the case with radiative outer boundary conditions and a constant densitized lapse. Again the result converges with resolution until about $t \sim 60M$ and simulations run longer for higher resolutions. However, this time a flat plateau forms only for a short time after the initial increase of Hamiltonian. For example for the highest resolution the curve is almost flat between $2M$ and $20M$. After that the Hamiltonian increases exponentially. This increase is the result of constraint violations entering through the outer boundary, since the radiative boundary conditions used here are not constraint preserving.

Figure 8 shows our results for the case of $1 + \log$ lapse together with radiative outer boundary conditions. The qualitative behavior in this case is the same as for the constant densitized lapse with radiative outer boundary conditions presented before in Fig. 7. Note, however, that the time axis has been extended since these runs last longer.

All plots were obtained for an angular resolution of $N_\theta = 14$ and $N_\phi = 13$. All we have done so far was to vary the radial resolution. Note that the Schwarzschild black hole evolved here is spherically symmetric. Thus, when the Cartesian components of our evolved variables are expanded in a Fourier series in θ or ϕ , only the three lowest frequencies contribute, so that only the first three complex coefficients can be non-zero. Since all our variables are real, the lowest coefficient must also be real. This implies that the first three complex coefficients can be described by five real numbers, which corresponds to five collocation points. Hence if we assume spherical symmetry throughout the evolution, a resolution of $N_\theta = N_\phi = 5$ would be entirely sufficient. Recall how-

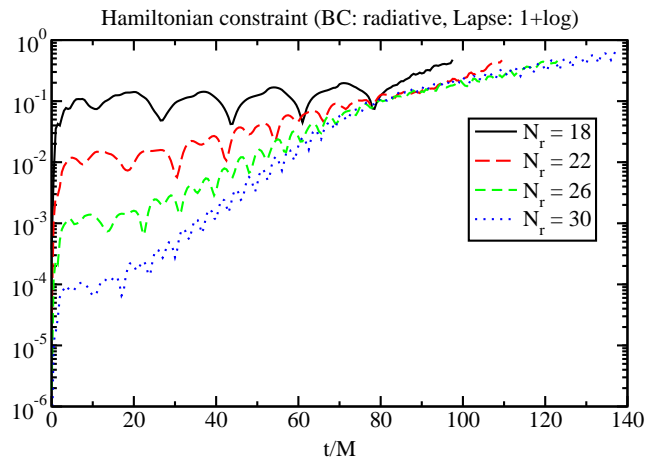


FIG. 8: The L^2 -norm of the normalized Hamiltonian constraint versus time for the case of radiative outer boundary conditions and a $1 + \log$ lapse. For increasing N_r the Hamiltonian converges until about $t \sim 60M$. The angular resolution is $N_\theta - 1 = N_\phi = 13$.

ever, that in order to avoid collocation points at the poles we require N_θ to be even, and thus the minimum we need is $N_\theta - 1 = N_\phi = 5$. If we run our simulations with this minimum angular resolution non-spherical modes are suppressed and our simulations run up to 50% longer than the ones shown above. Since our ultimate goal is to be able to also evolve non-spherically symmetric situations we have chosen not to do this. When we increase $N_\theta - 1 = N_\phi$ from 5 to a number between 6 and 10 we find that run-time decreases. Yet for values of $N_\theta \geq 14$ and $N_\phi \geq 13$ all results are largely independent of angular resolution. For this reason we have presented only results for $N_\theta - 1 = N_\phi = 13$.

Recall that in the case of finite differencing BSSN simulations with excision, instabilities were observed when a single black hole is evolved on a full grid [20]. These instabilities disappear when symmetries such as octant symmetry are imposed. In the present work no symmetries are imposed. This might be one reason for the observed instabilities. In fact, here we do not only evolve a full grid, but the full grid is also covered twice due to our use of Fourier expansions in both angles. This double covering corresponds to less symmetries than in usual full grid simulations. Thus one might worry that it could even lead to additional instabilities, above and beyond the full grid instability [20]. This is however not the case.

The double covering can be removed by using the fact that all evolved variables u have to satisfy

$$u(r, \theta, \phi) = u(r, 2\pi - \theta, \phi + \pi) = u(r, 2\pi - \theta, \phi - \pi) \quad (55)$$

if $\pi \leq \theta < 2\pi$. Thus if we use an even number of collocation points in both angles we can simply overwrite all variables at collocation points for which $\pi \leq \theta < 2\pi$ with their values at the corresponding points with $0 \leq \theta < \pi$, after each time step. Alternatively, one can also take the

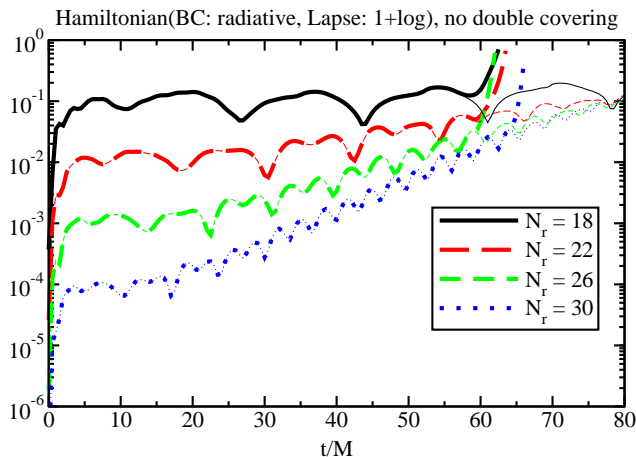


FIG. 9: The L^2 -norm of the normalized Hamiltonian constraint versus time for radiative outer boundary conditions and a $1 + \log$ lapse. The thick lines show how the Hamiltonian evolves when we remove the double covering (using Eq. (55)). For comparison the results with double covering (from Fig. 8) are shown as thin lines. When the double covering is removed the runs crash soon after convergence is lost (around $t \sim 60M$), while the runs with double covering carry on for a while with large errors and without converging. Note that in the convergent regime there is no noticeable difference between double covering and single covering, and both work equally well. The angular resolution is $N_\theta = N_\phi = 14$.

average of u at corresponding points and replace u at both points with this average. We have tried both methods to remove the double covering and both give the same result.

The thick lines in Fig. 9 show the time evolution of the Hamiltonian constraint for simulations where the double covering has been removed by using the averaging procedure described above, after each time step. For comparison the thin lines also depict the corresponding results with double covering. As one can see both single and double covering produce indistinguishable results until convergence is lost at around $60M$. After that the simulations with single covering blow up quickly, while the simulations with double covering continue for some time (see Fig. 8). However, after about $60M$ the simulations with double covering have large errors and do not converge any longer. Hence the effective runtime during which we get useful results is equal for both single and double covering. Thus we conclude that both single and double covering work equally well and that the double covering is not the reason for the observed instabilities in the BSSN evolutions described here.

Another way to remove the double covering would be to expand our variables in spherical harmonics instead of double Fourier expansions. This is, however, beyond the scope of this paper.

When working with spectral methods it is quite common to use filters to suppress instabilities. For example in the case of Fourier expansions one often used filter

consists of zeroing out the top most third of all spectral coefficients. This so called 2/3 rule can also be used for Chebyshev expansions. We would like to point out that no filters were used in the work presented above. We have, however, tested the simple 2/3 rule in our case and found that it has no effect on the observed instabilities. The only effect we observe is a reduced accuracy when the filters are on. This reduction is explained by the lower effective resolution when 1/3 of all coefficients is zeroed out.

IV. DISCUSSION

We have, for the first time, evolved the BSSN system by means of a pseudo-spectral collocation method. This method uses a grid of collocation points that are distributed over a spherical shell. On this grid we evolve the Cartesian components of all variables. We use Fourier expansions in both angles and a Chebyshev expansion in the radial direction. This double Fourier expansion leads to a double covering of the spherical shell in the sense that there are always two grid points which correspond to the same physical location in the shell. The fact that there are two corresponding points where all evolved variables must have the same value can also be used to undo the effects of the double covering after each evolution step. However, as we have seen in Sec. III, the simulations with single and double covering yield basically the same results in the convergent regime.

The BSSN system is second order in space, and we have implemented it as is, without any first order reductions. The main purpose of this work was to test this system together with boundary conditions and gauges that have so far only been used together with finite differencing methods. In particular, we use black hole excision and either radiative or constant outer boundary conditions. As gauges we have tested both $1 + \log$ lapse and constant densitized lapse. Depending on these choices we can evolve a single black hole in Kerr-Schild coordinates for about $100M$. After that the simulation crashes due to unstable exponentially growing modes. While this evolution time is not too impressive by today's standards, it demonstrates that most methods used in codes based on finite differencing can in principle also be used with spectral methods. In fact, our code tests with a non-linear wave equation show that both constant as well as radiative boundary conditions can be simply applied to all evolved fields without decomposing them into ingoing and outgoing modes. In this scalar wave case all our simulations are stable and no blowups were observed. Therefore it seems likely that the observed instabilities which occur with the BSSN system when we evolve a single black hole, are not caused by the simple radiative or constant outer boundary conditions used here. Rather the blowup may due to the use of black hole excision on a full grid without imposing any symmetries such as octant or bitant symmetry. Such a full grid instability has

also been observed in finite differencing implementations of BSSN [20] when excision is used. Indeed, we have not checked whether the version of the BSSN used here has some incoming modes (e.g. gauge modes) at the excision boundary. If such modes do exist, they require boundary conditions at the excision surface and our choice of not imposing any boundary conditions there may be the cause of the observed instabilities. We leave the study of such modes to future work.

We would also like to point out that the runtime of about $100M$ in the simulations described above, was achieved using the standard BSSN system without any parameter fine tuning. For example, it is well known that one can modify this system through the addition of constraints on the right hand side of the evolution equations. These additional terms can be multiplied by parameters which can be adjusted to extend the runtime. Recall that when the Einstein-Christoffel system [24] was first implemented [17] it ran for only about $40M$ before it crashed. By adding constraints with parameters this system was extended into what is now known as the KST system [17].

After parameter fine tuning this KST system was able to evolve single black holes for the much longer time of about $8000M$ [25]. It might be possible to extend the runtime of the BSSN simulations described in this work in an analogous way. Furthermore, the runtime and accuracy of our simulations should improve, if the simple constant or radiative boundary conditions used here are replaced by constraint preserving boundary conditions.

Acknowledgments

It is a pleasure to thank Bernd Brügmann, Marcus Ansorg, Mark Scheel and Lawrence Kidder for useful discussions about spectral methods. This work was supported by NSF grant PHY-0555644. We also acknowledge partial support by the National Computational Science Alliance under Grants PHY050012T, PHY050015N, and PHY050016N.

-
- [1] LIGO, IIGO - <http://www.ligo.caltech.edu/>.
 - [2] GEO, gEO600 - <http://www.geo600.uni-hannover.de/>.
 - [3] B. Schutz, *Class. Quantum Grav.* **16**, A131 (1999).
 - [4] T. W. Baumgarte and S. L. Shapiro, *Phys. Rev.* **D59**, 024007 (1999), gr-qc/9810065.
 - [5] F. Pretorius, *Class. Quant. Grav.* **22**, 425 (2005), gr-qc/0407110.
 - [6] F. Pretorius, *Phys. Rev. Lett.* **95**, 121101 (2005), gr-qc/0507014.
 - [7] F. Pretorius (2006), gr-qc/0602115, gr-qc/0602115.
 - [8] L. Lindblom, M. A. Scheel, L. E. Kidder, R. Owen, and O. Rinne (2005), gr-qc/0512093.
 - [9] M. A. Scheel et al. (2006), gr-qc/0607056.
 - [10] B. Brügmann, W. Tichy, and N. Jansen, *Phys. Rev. Lett.* **92**, 211101 (2004), gr-qc/0312112.
 - [11] M. Campanelli, C. O. Lousto, P. Marronetti, and Y. Zlochower, *Phys. Rev. Lett.* **96**, 111101 (2006), gr-qc/0511048.
 - [12] M. Campanelli, C. O. Lousto, and Y. Zlochower, *Phys. Rev.* **D73**, 061501 (2006), gr-qc/0601091.
 - [13] M. Campanelli, C. O. Lousto, and Y. Zlochower (2006), gr-qc/0604012, gr-qc/0604012.
 - [14] J. G. Baker, J. Centrella, D.-I. Choi, M. Koppitz, and J. van Meter, *Phys. Rev. Lett.* **96**, 111102 (2006), gr-qc/0511103.
 - [15] J. G. Baker, J. Centrella, D.-I. Choi, M. Koppitz, and J. van Meter, *Phys. Rev.* **D73**, 104002 (2006), gr-qc/0602026.
 - [16] J. G. Baker et al. (2006), astro-ph/0603204, astro-ph/0603204.
 - [17] L. E. Kidder, M. A. Scheel, and S. A. Teukolsky, *Phys. Rev. D* **64**, 064017 (2001), gr-qc/0105031.
 - [18] C. Gundlach and J. M. Martin-Garcia, *Phys. Rev.* **D70**, 044031 (2004), gr-qc/0402079.
 - [19] A. Arbona, C. Bona, J. Massó, and J. Stela, *Phys. Rev. D* **60**, 104014 (1999), gr-qc/9902053.
 - [20] M. Alcubierre and B. Brügmann, *Phys. Rev. D* **63**, 104006 (2001), gr-qc/0008067.
 - [21] H.-J. Yo, T. W. Baumgarte, and S. L. Shapiro, *Phys. Rev. D* **66**, 084026 (2002).
 - [22] U. Sperhake, K. L. Smith, B. Kelly, P. Laguna, and D. Shoemaker, *Phys. Rev.* **D69**, 024012 (2004), gr-qc/0307015.
 - [23] R. M. Wald, *General Relativity* (The University of Chicago Press, Chicago, 1984), ISBN 0-226-87032-4 (hardcover), 0-226-87033-2 (paperback).
 - [24] A. Anderson and J. W. York, *Phys. Rev. Lett.* **82**, 4384 (1999), gr-qc/9901021.
 - [25] M. A. Scheel, L. E. Kidder, L. Lindblom, H. P. Pfeiffer, and S. A. Teukolsky, *Phys. Rev. D* **66**, 124005 (2002), gr-qc/0209115.